Lanthanide-doped inorganic nanoparticles turn molecular triplet excitons bright

Sanyang Han[1#], Renren Deng[1,2#*], Qifei Gu[1], Limeng Ni[1], Uyen Huynh[1], Jiangbin Zhang[1,3], Zhigao Yi[4], Baodan Zhao[1,5], Hiroyuki Tamura[6], Anton Pershin[7], Hui Xu[8], Zhiyuan Huang[9], Shahab Ahmad[10], Mojtaba Abdi-Jalebi[1], Aditya Sadhanala[1], Ming Lee Tang[9], Artem Bakulin[3], David Beljonne[7], Xiaogang Liu[4,11*] and Akshay Rao[1*]

[1]Cavendish Laboratory, University of Cambridge, Cambridge CB3 0HE, United Kingdom.
[2]Institute for Composites Science Innovation, School of Materials Science and Engineering, Zhejiang University, Hangzhou, 310027, China.
[3]Department of Chemistry, Imperial College London, London SW7 2AZ, United Kingdom.
[4]Department of Chemistry, National University of Singapore, Singapore 117543, Singapore.
[5]State Key Laboratory of Modern Optical Instrumentation, College of Optical Science and Engineering, International Research Center for Advanced Photonics, Zhejiang University, Hangzhou, 310027, China.
[6]Department of Chemical System Engineering, The University of Tokyo, Tokyo, 113-8656, Japan.
[7]Laboratory for Chemistry of Novel Materials, University of Mons, Place du Parc 20, B-7000, Mons, Belgium.
[8]School of Chemistry and Material Science, Heilongjiang University, Harbin 150080, China.
[9]Department of Chemistry, University of California, Riverside, CA, 92521, USA.
[10]Department of Physics, Indian Institute of Technology Jodhpur, Karwar, Jodhpur- 342037, India.
[11]The N.1 Institute for Health, National University of Singapore, Singapore 117456, Singapore.

[#]These authors contributed equally to this work.

*Correspondence author. Email: ar525@cam.ac.uk (A.R.), chmlx@nus.edu.sg (X.L.), rdeng@zju.edu.cn (R.D.)

The generation, control and transfer of triplet excitons in molecular and hybrid systems is of great interest due to their long lifetime and diffusion length in both solid-state and solution phase systems, and due to their applications in light emission[1], optoelectronics[2,3], photon frequency conversion[4,5] and photocatalysis[6,7]. Molecular triplet excitons are 'dark states' due to the forbidden nature of the direct optical transition between the spin-0 ground state and the spin-1 triplet levels[8]. Hence, conventionally triplet dynamics are controlled through heavy-metal based spin-orbit coupling[9-11] or control of the singlet-triplet energy splitting[12,13] via molecular design. Both these methods place constraints on the range of properties that can be controlled and the molecular structures that can be used. Here, we demonstrate that it is possible to control triplet dynamics by coupling organic molecules to lanthanide-doped inorganic insulating nanoparticles. This allows the classically forbidden $S_0 \rightarrow T_n$ transitions to gain oscillator strength, enabling triplets to be directly generated on molecules via photon absorption. Photogenerated singlet excitons can be converted to triplet excitons on sub-10 ps timescales with unity efficiency by inter-system crossing. Triplet exciton states of the molecules can undergo energy transfer to the lanthanide ions with unity efficiency, which allows us to achieve luminescent harvesting of the dark triplet excitons. Furthermore, the triplet excitons generated in the lanthanide nanoparticle-molecule hybrid systems by NIR photoexcitation can undergo efficient upconversion via an unprecedented lanthanide-triplet excitation fusion process that enables endothermic upconversion and allows for efficient NIR to visible upconversion in the solid state. These results provide a new paradigm to control triplet excitons, a capability that is essential for many fields of optoelectronic and biomedical research.

Figure 1a shows a schematic of lanthanide-doped nanocrystals ($NaLnF_4$) and the structures of some of the model molecules used in our study (rubrene and tetracene derivatives), along with their triplet energies. Unlike semiconductor quantum dots (QDs), these lanthanide-doped nanocrystals are insulators and their optoelectronic properties are governed solely by the lanthanide ions. We begin by preparing blended films of rubrene with $NaGdF_4$ nanocrystals by drop-casting (Supplementary Figs. 1 and 2).

Figure 1b shows the absorption spectra, measured by photothermal deflection spectroscopy (PDS), of a $NaGdF_4$-rubrene blend film, a pristine rubrene film and a pure $NaGdF_4$ film. Apart from the typical absorption features associated with the $S_0 \rightarrow S_n$ transitions in rubrene, we observe new absorption features between 700-1100 nm in the $NaGdF_4$-rubrene blend film. In contrast, the pristine rubrene and $NaGdF_4$ films have no absorption in the same region. Significantly, the spectra reveal a ~ 200 fold enhancement in the near-infrared (NIR) absorbance of the $NaGdF_4$-rubrene blend compared with the pristine rubrene film. To understand this observation, we performed Density Functional Theory (DFT) and MultiReference second-order Møller-Plesset perturbation theory (MRMP2) calculations (See Supplementary Section 2). We found that the experimentally measured absorption in the NIR region (800-1100 nm) matches well with the calculated absorption for the $S_0 \rightarrow T_1$ transition of an isolated rubrene molecule (Fig. 1b, inset). Note that theoretical prediction for the 0-0 transition shows a much higher intensity. We attributed this suppression of the 0-0 band to the Herzberg-Teller (HT) mechanism, as described previously[14]. The extra absorption in the $NaGdF_4$-rubrene blend film is thus assigned to the $S_0 \rightarrow T_n$ transition of rubrene, implying that the usually dark $S_0 \rightarrow T_n$ transition has become bright in the blended system. Similarly, the enhanced dark $S_0 \rightarrow T_n$ transition feature was also observed in tetracene derivatives based blends (Supplementary Fig. 3).

One explanation for the enhanced $S_0 \rightarrow T_n$ absorption could be related to the spin-orbit coupling (SOC) associated with the presence of heavy atoms (Z = 64 for Gd). To test this hypothesis, we prepared blended films of rubrene with different types of lanthanide-doped nanoparticles, including $NaGdF_4$, $NaYF_4$ and $NaLuF_4$. Gd^{3+} (Z = 64) has seven unpaired 4f electrons[15], while Y^{3+} (Z = 39) and Lu^{3+} (Z = 71) have zero spin momentum (Supplementary Data Table 1). The absorption of the $S_0 \rightarrow T_n$ transition was only observed in the blends with non-zero spin, while no features could be observed for the Y^{3+}- and Lu^{3+}-based blends despite the higher atomic mass of Lu^{3+} (Fig. 1b). These results suggest that the enhanced $S_0 \rightarrow T_n$ transition is not due to the heavy atom-induced SOC but related to the spins of unpaired 4f electrons of lanthanide ions.

To further probe the nature of the coupling between organic molecules and lanthanide nanocrystals, we prepared lanthanide nanoparticles modified with a series of carboxylic acid-functionalized tetracene derivatives, 5-carboxylic acid tetracene (5-CT), 4-(tetracen-5-yl)benzoic acid (CPT) and 4'-(tetracen-5-yl)-[1,1'-biphenyl]-4-carboxylic acid (CPPT), as shown in Fig. 1a. These molecules can selectively bind to surface cations of the nanocrystals through their carboxylic groups. The different spacer groups allow us to control the distance between lanthanide ions and the tetracene core, where the triplet excitons will be localized. We studied blended films of 5-CT with different $NaLnF_4$ (Ln = Gd^{3+}, Er^{3+}, Y^{3+}, or Lu^{3+}) nanocrystals, as shown in Fig. 1c. The absorption spectra showed that all the lanthanides with unpaired 4f electrons (Gd^{3+} and Er^{3+}) give rise to an enhanced NIR absorption of 5-CT molecules, while the lanthanides without unpaired electron (Y^{3+} and Lu^{3+}) have a neglectable effect. Figure 1d compares the effect of longer spacer group. As we move from 5CT to CPT and CPPT, it was observed that the absorption in the NIR spectral region decreases. This

result confirms that the coupling between lanthanides and tetracene molecules is very sensitive to the distance between them. Based on these observations, we propose that the proximity of the organic molecules to the lanthanide ions with unpaired spins permits photon absorption to directly generate triplet states, $S_0 \rightarrow T_n$. We return to the nature of this interaction later.

We next explore the effect of the lanthanide ions on the excited states of the organic semiconductors. We chose 9-[3-carboxyl-4-(diphenylphosphinoyl)phenyl]-9H-carbazole (CPPOA) as a model molecule due to its high lying triplet state (which will be important for the discussion of energy transfer below). We prepared colloidal solutions of $NaYF_4$@$NaLnF_4$ core-shell nanoparticles with surface-bound CPPOA molecules (Fig. 2a) and studied the dynamics of photoexcitations using pump-probe spectroscopy. The S_1 state of CPPOA on the $NaYF_4$@$NaGdF_4$ nanoparticle was found to decay with a time constant of 82 ps (Fig. 2b), concomitant with the rise time of the triplet excitons (T_1, 97 ps). This indicates that the photogenerated singlet of CPPOA attached to the $NaYF_4$@$NaGdF_4$ nanoparticles undergoes rapid intersystem crossing (ISC). In contrast, the singlet on the pristine CPPOA shows a decay time of 12.9 ns with a concomitant triplet rise over 18.4 ns. Thus, the presence of the Gd^{3+}-based nanoparticles increases the rate of the ISC by three orders of magnitude (Fig. 2c). To probe this further, we attached CPPOA to a series of $NaYF_4$@$NaLnF_4$ core-shell nanoparticles with different lanthanide ions in the shell and measured the triplet generation rate. As shown in Fig. 2d, we observe an enhanced ISC rate for nanoparticles with unpaired 4f electrons (Tb^{3+}, Eu^{3+}, Gd^{3+} and Yb^{3+}), but not for those with no unpaired spins (Y^{3+} and Lu^{3+}) (Supplementary Tables 1-3). The same trend was observed in sub-gap absorption enhancement for CPPOA-capped nanoparticles, analogous to the results in Fig. 1 (Supplementary Figs. 9 and 10a). For Eu^{3+}-doped nanoparticles, we measured a triplet rise time of 9.3 ps, which is 1978 times faster than that of the pristine CPPOA molecules. The

ISC efficiency is estimated to be 99.4 %, based on the singlet lifetime quenching. Thus, in addition to turning $S_0 \rightarrow T_n$ transitions bright, the interaction between the CPPOA and the unpaired spins on the lanthanide nanoparticles also yields highly efficient ISC (ref. 16; see Supplementary Figs. 11-32 for full details).

It can be seen in Fig. 2d that the fast rise of the T_1 state for Tb^{3+}- and Eu^{3+}- containing nanoparticles is accompanied by a quick decay of the T_1 state (883 ps for Eu^{3+} and 7.66 ns for Tb^{3+}). This decay is caused by the transfer of the T_1 state from CPPOA to the $^5D_1/^5D_0$ and $^5D_4$ levels of Eu^{3+} and Tb^{3+}, respectively (Fig. 3a). Based on the quenching of the triplet lifetime, the calculated quantum efficiency of triplet energy transfer from CPPOA to lanthanide nanoparticles exceeds 99%. This near quantitative triplet energy transfer gives rise to bright luminescence from the lanthanide ions upon excitation of the coupled systems at 365 nm (Fig. 3b and Supplementary Fig. 10b, 33-35). These results show that molecular triplet excitons can be efficiently transferred to lanthanide-doped nanoparticles, allowing the luminescent harvesting of normally dark triplet excitons.

This luminescent harvesting of triplet excitons is not restricted to triplets generated by the ISC on the surface of the nanoparticles but also from other processes such as singlet fission. Tetracene and rubrene are both well-known singlet fission materials, where the photogenerated singlet excitons rapidly and efficiently convert to a pair of triplet excitons[13,17]. Fig. 3c shows data for blend films of tetracene and rubrene with $NaGdF_4$:Yb (50 mol%) nanoparticles. These nanoparticles feature an energy gap of 1.25 eV between the lowest excited state ($^2F_{5/2}$) and the ground state ($^2F_{7/2}$) of Yb^{3+}, which lies near the triplet energy of tetracene (1.25 eV; ref. 17) and above that of rubrene (1.14 eV; ref. 18). When a $NaGdF_4$:Yb-tetracene blend film was excited at 405 nm, we recorded a strong

quenching of the characteristic visible emission from tetracene in favour of a Yb^{3+} emission located at 950-1100 nm (Fig. 3c and Supplementary Fig. 36). This emission quenching arises from triplet-mediated energy transfer from tetracene to Yb^{3+}, as the emission of Yb^{3+} in the blend is highly sensitive to oxygen (Supplementary Fig. 37). Magnetic field-dependent photoluminescence measurements showed an increase in emission from the tetracene while the emission from Yb^{3+} decreased with increasing magnetic field[19,20], confirming the transfer of triplets generated by the singlet fission process to Yb^{3+} (Supplementary Figs. 44-46). In contrast, almost no quenching of the visible and no NIR emission was observed in the rubrene blend owing to inefficient triplet energy transfer to Yb^{3+}.

Figure 4a shows the photoluminescence spectra of the $NaGdF_4$:Yb-rubrene and $NaGdF_4$:Yb-tetracene blends upon 980-nm excitation. Spectra corresponding to the singlet emission from both tetracene and rubrene were obtained, consistent with the upconversion of absorbed energy. This upconverted emission is visible even under ambient light conditions (Supplementary Fig. 38) and found to have a quadratic dependence on the excitation power at low excitation fluence, followed by a slope change from 2 to 1 at higher excitation density (Supplementary Fig. 39).

Considering the broadband absorption of the sample in the NIR wavelength region (Supplementary Fig. 40), we carried out excitation in a spectral range from 850 to 1020 nm and observed upconverted emission at all excitation wavelengths (Supplementary Figs. 41 and 42). These results suggest that the interaction between the molecular triplet exciton with the lanthanide, rather than the conventional triplet-triplet annihilation (TTA) process[21-23], mediates the upconversion process in organic molecules after triplet transfer from photoexcited Yb^{3+}-doped nanoparticles under

NIR irradiation (Fig. 4b). To further investigate the upconversion mechanism, we prepared a series of blends with varying concentration ratios of $NaGdF_4$:Yb and rubrene or tetracene. The main emission peak shifted from 540 (2.29 eV) to 480 nm (2.58 eV) for the $NaGdF_4$:Yb-tetracene blends when the concentration ratio of tetracene to nanoparticle was changed from 10:1 to 1:100 (Fig. 4c and Supplementary Fig. 43 for rubrene blends). Interestingly, an emission characteristic of a single tetracene molecule[24] was obtained when the concentration of tetracene was diluted to 1 molecule per 100 nanoparticles. This upconverted emission is recorded at room temperature with moderate excitation density (< 10 W/cm^2). This is in stark contrast to the conventional two-photon absorption methods for generating anti-Stokes emission from single molecules, which require a significantly higher excitation density (> 10^6 W/cm^2). Conventional TTA upconversion through bimolecular triplet-triplet states does not enable the single molecular emission of tetracene because the emission would be shifted to lower energies due to excitonic coupling, as happens when we increase the tetracene concentration in the blend films. This again suggests that the upconverted emission is produced by a different process. Magnetic field-dependent photoluminescence studies show no change in upconverted emission under applied magnetic field (Supplementary Fig. 47), confirming that the upconversion process is not mediated by the TTA (see Supplementary Section 9 and Figs. 48-49 for full details).

Given that the singlet energy of tetracene (for a single molecule, 2.62 eV; Supplementary Figs. 48 and 50) is higher than the total energy contained in two excitation photons (1.25 eV × 2 = 2.50 eV), this new mechanism enables us to obtain endothermic upconversion. To investigate this endothermic upconversion process further, we performed temperature-dependent upconversion measurements. The upconversion emission intensity for the 1:100 film gradually increased as the temperature

reached 80 K, presumably due to the suppression of non-radiative loss channels at low temperatures (Fig. 4d). However, further lowering the temperature resulted in a decrease in upconversion emission (Supplementary Figs. 51 and 52). We note that the downshifting luminescence of the same sample under 405 nm excitation increases monotonically as the temperature drops, and the integrated emission intensity at 20 K is 12 times stronger than that measured at room temperature (Supplementary Fig. 53).

At room temperature, we measured an internal photoluminescence quantum yield (PLQY) of more than 1% for the $NaGdF_4$:Yb-rubrene blend film with moderate excitation of > 16 W/cm^2. A maximum PLQY value of 1.9 ± 0.5 % reached at an irradiance power density of 75 W/cm^2 (Fig. 4e). Note that the singlet PLQY of rubrene in the blend under 405 nm excitation at room temperature was measured to be 20 ± 2.1 %. This suggests a maximum singlet yield of ~ 10 % per absorbed NIR photon for the $NaGdF_4$:Yb-rubrene. A maximum PLQY value of 16.2 ± 3.4 % was attained at 10 K (Supplementary Fig. 54), due to reduction of the non-radiative energy loss pathways at low temperatures. Given the fact that two lower-energy photons are converted to one higher-energy photon during the upconversion process, our system has thus converted ~ 32 % of the absorbed photons.

In comparison with the conventional lanthanide[25-28] or TTA[5,22] based upconversion, a key feature of the lanthanide-triplet excitation fusion approach demonstrated here is that the excitation energy can be directly amassed in both organic and inorganic components without the need for a sensitization step. Therefore, energy loss during the sensitization process can be effectively reduced to zero[29]. In addition, lanthanide-doped nanoparticles have no absorption at higher energies, thereby

eliminating the problem of reabsorption associated with quantum dots/molecules systems[30,31]. Furthermore, due to nature of the spin states, normal spin statistical limitations that apply to the conventional TTA, do not apply to the lanthanide-triplet upconversion.

In conclusion, we have demonstrated that it is possible to control and manipulate triplet excitons dynamics by coupling conventional molecular systems to the unpaired spins of lanthanide ions doped in inorganic nanoparticles. Further experimental and theoretical work is called for to understand the nature of coupling in these systems. Our results up new avenues for triplet sensitization, photocatalysis, optoelectronics, sensing, and photon frequency conversion driven by optically bright triplet excitons.

Online content

Any methods, additional references, Nature Research reporting summaries, source data, extended data, supplementary information, acknowledgements, peer review information; details of author contributions and competing interests; and statements of data and code availability are available at https://doi.org/xxx.

References

1. Bolton, O., Lee, K., Kim, H. J., Lin, K. Y. & Kim, J. Activating efficient phosphorescence from purely organic materials by crystal design. *Nat. Chem.* **3**, 205-210 (2011).
2. Baldo, M. A. et al. Highly efficient phosphorescent emission from organic electroluminescent devices. *Nature* **395**, 151-154 (1998).
3. Uoyama, H., Goushi, K., Shizu, K., Nomura, H. & Adachi, C. Highly efficient organic light-emitting diodes from delayed fluorescence. *Nature* **492**, 234-238 (2012).

4. Yanai, N. & Kimizuka, N. New triplet sensitization routes for photon upconversion: thermally activated delayed fluorescence molecules, inorganic nanocrystals, and singlet-to-triplet absorption *Acc. Chem. Res.* **50**, 2487–2495 (2017).
5. Schulze, T. F. & T. W. Schmidt, Photochemical upconversion: present status and prospects for its application to solar energy conversion. *Energy Environ. Sci.* **8**, 103-125 (2015).
6. Ravetz, B. D. et al. Photoredox catalysis using infrared light via triplet fusion upconversion. *Nature* **565**, 343-346 (2019).
7. Mongin, C., Garakyaraghi, S., Razgoniaeva, N., Zamkov, M. & Castellano, F. N. Direct observation of triplet energy transfer from semiconductor nanocrystals. *Science* **351**, 369-372 (2016).
8. Kohler, A. & Bassler, H. Triplet states in organic semiconductors. *Mater. Sci. Eng. R* **66**, 71-109 (2009).
9. Lamansky, S. et al. Highly phosphorescent bis-cyclometalated iridium complexes: synthesis, photophysical characterization, and use in organic light emitting diodes. *J. Am. Chem. Soc.* **123**, 4304-4312 (2001).
10. Bünzli, J.-C. G. On the design of highly luminescent lanthanide complexes. *Coord. Chem. Rev.* **293–294**, 19–47 (2015).
11. Klink, S. I., Kerizer, H. & van Veggel, F. C. J. M. Transition metal complexes as photosensitizers for near-infrared lanthanide luminescence. *Angew. Chem. Int. Ed.* **39**, 4319-4321 (2000).
12. Penfold, T. J., Gindensperger, E., Daniel, C. & Marian, C. M. Spin-vibronic mechanism for intersystem crossing. *Chem. Rev.* **118**, 6975-7025 (2018).
13. Smith, M. B. & Michl, J. Singlet fission. *Chem. Rev.* **110**, 6891-6936 (2010).
14. Wykes, M., Parambil, R., Beljonne, D. & Gierschner, J. Vibronic coupling in molecular crystals: a Franck-Condon Herzberg-Teller model of H-aggregate fluorescence based on quantum chemical cluster calculations Vibronic coupling in molecular crystals. *J. Chem. Phys.* **143**, 114116 (2015).
15. Auzel, F. Upconversion and anti-stokes processes with f and d ions in solids. *Chem. Rev.* **104**, 139-174 (2004).
16. Tobita, S., Arakawa, M. & Tanaka, I. The paramagnetic metal effect on the ligand localized $S_1 \rightarrow T_1$ intersystem crossing in the rare-earth-metal complexes with methyl salicylate. *J. Phys. Chem.* **89**, 5649-5654 (1985).

17. Tiberghien, A. & Delacote, G. Evaluation of the crystalline tetracene triplet davydov splitting. *Chem. Phys. Lett.* **8**, 88-90 (1971).
18. Tao, S. et al. Optical pump-probe spectroscopy of photocarriers in rubrene single crystals. *Phys. Rev. B* **83**, 075204 (2011).
19. Thompson, N. J. et al. Energy harvesting of non-emissive triplet excitons in tetracene by emissive PbS nanocrystals. *Nat. Mater.* **13**, 1039-1043 (2014).
20. Tabachnyk, M. et al. Resonant energy transfer of triplet excitons from pentacene to PbSe nanocrystals. *Nat. Mater.* **13**, 1033-1038 (2014).
21. Wu, M. et al. Solid-state infrared-to-visible upconversion sensitized by colloidal nanocrystals. *Nat. Photon.* **10**, 31-34 (2016).
22. Zhao, J., Ji, S. & H. Guo, Triplet–triplet annihilation based upconversion: from triplet sensitizers and triplet acceptors to upconversion quantum yields. *RSC Adv.* **1**, 937-950 (2011).
23. Singh-Rachford, T. N. & Castellano, F. N. Photon upconversion based on sensitized triplet–triplet annihilation. *Coord. Chem. Rev.* **254**, 2560-2573 (2010).
24. Burdett, J. J., Müller, A. M., Gosztola, D. & Bardeen, C. J. Excited state dynamics in solid and monomeric tetracene: The roles of superradiance and exciton fission. *J. Chem. Phys.* **133**, 144506 (2010).
25. Zhao, J. et al. Single-nanocrystal sensitivity achieved by enhanced upconversion luminescence *Nat. Nanotechnol.* **8**, 729–734 (2013).
26. Haase, M. & Schäfer, H. Upconverting nanoparticles. *Angew. Chem. Int. Ed.* **50**, 5808-5829 (2011).
27. Garfield, D. J. et al. Enrichment of molecular antenna triplets amplifies upconverting nanoparticle emission. *Nat. Photon.* **12**, 402-407 (2018).
28. Pollnau, M., Gamelin, D. R., Lüthi, S. R., Güdel, H. U. & Hehlen, M. P. Power dependence of upconversion luminescence in lanthanide and transition-metal-ion systems. *Phys. Rev. B* **61**, 3337-3346 (2000).
29. Nienhaus, L., Wu, M., Bulović, V., Baldo, M. A. & Bawendi, M. G. Using lead chalcogenide nanocrystals as spin mixers: a perspective on near-infrared-to-visible upconversion. *Dalton Trans.* **47**, 8509-8516 (2018).
30. Nienhaus, L. et al. Speed limit for triplet-exciton transfer in solid-state PbS nanocrystal-sensitized photon upconversion. *ACS Nano* **11**, 7848-7857 (2017).

31. Huang, Z. et al. Hybrid molecule−nanocrystal photon upconversion across the visible and near-infrared. *Nano Lett.* **15**, 5552−5557 (2015).

Fig. 1 | Lanthanide nanocrystal-coupled triplet excitation. **a**, Schematic illustration of a lanthanide-doped nanocrystal ($NaLnF_4$) and the organic molecules in our study. **b**, Comparison of the PDS spectra of films of $NaGdF_4$ (GdNCs)-rubrene, $NaLuF_4$ (LuNCs)-rubrene, $NaYF_4$ (YNCs)-rubrene with pristine rubrene and neat GdNCs. Only the system in which the lanthanide has unpaired spin i.e. the $NaGdF_4$ (GdNCs)-rubrene films show a broadband absorption from 700 to 1100 nm, and the inset shows that this absorption matches the calculated direct transition from the ground singlet state (S_0) to the lowest triplet state (T_1). **c**, Comparison of absorption spectra of 5-CT coupled with various lanthanide nanoparticles, including $NaGdF_4$ (GdNCs), $NaErF_4$ (ErNCs), $NaLuF_4$ (LuNCs), and $NaYF_4$ (YNCs). Enhanced NIR absorption, related to the direct excitation of triplets, is only observed in the presence of lanthanide ions with unpaired spins (Gd^{3+} and Er^{3}) **d**, Comparison of absorption spectra of GdNCs coupled with tetracene derivatives (5-CT, CPT, CPPT). The enhanced NIR absorption decreases with increasing spacing between the lanthanide nanoparticle and the core of the molecule.

Fig. 2 | Ultrafast intersystem crossing in organic molecules coupled to lanthanide-doped nanoparticles. **a**, Schematic illustration of a $NaYF_4$@$NaLnF_4$ core-shell nanoparticle modified with CPPOA. **b**, The extracted kinetics showing the singlet (S_1) decay and triplet (T_1) rise of a solution containing pristine CPPOA molecules and a solution of CPPOA-modified $NaYF_4$@$NaGdF_4$ nanoparticles. The singlet lifetime decreases from 12.9 ns in the pristine CPPOA to 82.3 ps in CPPOA-modified $NaYF_4$@$NaGdF_4$, indicating greatly enhanced intersystem crossing (ISC). **c**, the interaction between the lanthanides and the molecules accelerates the ISC from the singlet to triplet exciton states of the molecule. **d**, Kinetics of triplet generation and decay in the CPPOA molecules attached to different types of core-shell nanoparticles. The compositions of the core-shell nanoparticles are $NaYF_4$@$NaEuF_4$, $NaYF_4$@$NaGdF_4$, $NaYF_4$@$NaTbF_4$, $NaYF_4$@$NaYbF_4$, $NaYF_4$@$NaLuF_4$, and $NaYF_4$@$NaYF_4$. For lanthanides with unpaired 4f electrons (Tb^{3+}, Eu^{3+}, Gd^{3+} and Yb^{3+}) enhanced ISC is seen, while those with no unpaired spins (Y^{3+} and Lu^{3+}) show no obvious enhancement in ISC. In addition, an enhanced triplet decay (7.66 ns and 883 ps) of CPPOA on the nanoparticles containing Tb^{3+} or Eu^{3+} suggests triplet energy transfer to the lanthanide ions.

Fig. 3 | Triplet energy transfer from molecules to nanoparticles. **a**, Simplified energy diagram showing the triplet energy transfer (TET) from the molecular triplet state to lanthanide emitters (Ln^{3+}) following a fast intersystem crossing (ISC) or singlet fission (SF) process. **b**, Photoluminescence spectra and corresponding luminescence photos of colloidal solutions containing CPPOA-modified

$NaYF_4$@$NaTbF_4$ and $NaYF_4$@$NaEuF_4$ nanoparticles under excitation at 365 nm. **c**, Photoluminescence spectra of $NaGdF_4$:Yb-tetracene and $NaGdF_4$:Yb-rubrene blend films excited at 405 nm. Luminescence arises from the transfer of triplet excitons generated via singlet fission to the $^2F_{5/2}\rightarrow{}^2F_{7/2}$ transition of Yb^{3+}. The process is inefficient in rubrene due to its triplet energy being lower than the $^2F_{5/2}\rightarrow{}^2F_{7/2}$ transition of Yb^{3+} (1.14 vs 1.25 eV).

Fig. 4 | Lanthanide-triplet exciton fusion (LTF) upconversion in nanoparticle-molecule blends. a, Photoluminescence spectra of $NaGdF_4$:Yb-tetracene (50:1) and $NaGdF_4$:Yb-rubrene (1:10) blend films excited at 980 nm (~40 W/cm^2), showing upconverted emission arising from the singlet state of the organics. **b**, Proposed lanthanide-triplet exciton fusion upconversion process. **c**, Upconversion spectra and corresponding emission photographs of $NaGdF_4$:Yb-tetracene blend films with varying nanocrystal-to-tetracene ratios in the films. **d**, The plot of the temperature-dependent upconversion emission (integrated from 475 to 650 nm) of the $NaGdF_4$:Yb-tetracene blend films (tetracene: $NaGdF_4$:Yb = 1:100) **e**, The internal quantum yield (PLQY) of the $NaGdF_4$:Yb-rubrene blend measured as a function of excitation power density (excitation at 980nm). (Inset) Temperature-dependent quantum yield of the same sample under excitation of 980 nm for a power density of 76 W/cm^2.

Methods

Materials

$Gd(CH_3CO_2)_3$•xH_2O (99.9%), $Y(CH_3CO_2)_3$•xH_2O (99.9%), $Yb(CH_3CO_2)_3$•$4H_2O$ (99.9%), $Tb(CH_3CO_2)_3$•xH_2O (99.9%), $Eu(CH_3CO_2)_3$•xH_2O (99.9%), $Lu(CH_3CO_2)_3$•xH_2O (99.9%), NaOH (98+%), NH_4F (99%), 1-octadecene (90%), oleic acid (90%), Rubrene (99.99%), Tetracene (99.99%), and all anhydrous solvents were purchased from Sigma-Aldrich. If not stated otherwise, all chemicals were used as received without further purification.

Procedure for the synthesis of lanthanide (Ln)-doped $NaLnF_4$ nanocrystals (NCs)

The lanthanide nanocrystals were synthesized according to a well-documented co-precipitation method[32]. In a typical experiment for synthesizing 5-nm $NaGdF_4$:Yb (50 mol%) nanocrystals, a water solution (2 mL) containing $Gd(CH_3CO_2)_3$ (0.2 mmol) and $Yb(CH_3CO_2)_3$ (0.2 mmol) were mixed with oleic

acid (3.5 mL) and 1-octadecene (10.5 mL) in a 50-mL flask, followed by heating to 150 ˚C for 2 h. Thereafter, the reactant was cooled down to 50 ˚C, and a methanol solution (6 mL) containing NH_4F (1.36 mmol) and NaOH (1 mmol) was added. The mixed solution was stirred for 30 min. The reaction temperature was then raised to 100 ˚C to remove the methanol from the reaction solution. After that, the reactant was heated to 270 ˚C under a nitrogen atmosphere for 1 h, followed by cooling down to room temperature. The resulted nanocrystals were extracted through repeated precipitation with a mixture of ethanol and methanol, collected by centrifugation at 4000 rpm for 5 min, and re-dispersed in 4 mL of hexane. The pure $NaGdF_4$ and $NaYF_4$ nanocrystals were synthesized with the same procedure with the addition of corresponding $Ln(CH_3CO_2)_3$ solution.

Procedure for the synthesis of $NaYF_4$ core nanoparticles

In a typical procedure[32], an aqueous solution of $Y(CH_3CO_2)_3 \bullet xH_2O$ (2 mL, 0.2 M) was mixed with 3 mL of oleic acid (OA) in a 50 mL flask. The mixture was heated at 150 ^oC in an oil bath and kept for 30 min. Then 7 mL of 1-octadecene (ODE) were added to the flask. The mixture was cooled to 50 ^oC after 30 min. After that, a methanol solution (6 mL) containing NH_4F (1.6 mmol) and NaOH (1 mmol) was then added to the core precursor and stirred continuously for 30 min. After the removal of the low boiling point solvent, the temperature was increased to 290 ^oC under the argon atmosphere. After 2 h, the mixture was cooled down and washed by ethanol several times. The product was re-dispersed in 4 mL of cyclohexane.

Procedure for the Synthesis of $NaYF_4$@$NaLnF_4$ (Ln = Y, Gd, Eu, Tb, Yb, Lu) core-shell nanoparticles

$NaLnF_4$ shell precursor was then prepared by adding an aqueous solution of $Ln(CH_3CO_2)_3 \bullet xH_2O$ (1 mL, 0.2 M, Ln = Y, Gd, Eu, Tb, Yb, Lu) into the mixture of OA (3 mL) and ODE (7 mL). The mixture was heated at 150 ^oC in an oil bath for 1 h. After cooling down to 80 ^oC, $NaYF_4$ core nanoparticles in 4 mL of cyclohexane were added, and the resulting mixture was kept at 80 ^oC for 30 min. Subsequently, a methanol solution of NH_4F (0.8 mmol) and NaOH (0.5 mmol) were added under magnetic stirring and kept for 30 min at 50 ^oC. After that, the temperature was increased to 100 ^oC to evaporate the low boiling point solvents. The mixture was finally heated at 290 ^oC under argon atmosphere for 2 h. After

cooling to room temperature, the product nanoparticles were precipitated, washed several times with ethanol, and re-dispersed in 4 mL of cyclohexane for further use.

Preparation of ligand-free lanthanide nanocrystals

The as-prepared oleic acid-capped nanoparticles were precipitated from the hexane solution by adding acetone and then redispersed in an acetone solution containing HCl (0.1 M). The solution was ultrasonicated for 20 min to remove the oleate ligands on the surface. After the reaction, the nanocrystals were collected by centrifugation. The precipitants were washed with acetone/methanol several times and finally redispersed in methanol[33].

Nanoparticle-molecule film fabrication

Samples were fabricated on 15-mm round glass substrates. In a typical experiment, the glass substrates were first cleaned by sequential sonication in isopropanol and acetone, followed by treating with oxygen plasma for 10 min. The substrates were then transferred to a nitrogen glovebox. An anhydrous chloroform solution of tetracene or rubrene was mixed with the methanol solution of nanoparticles in the glovebox. The resulted organic-nanocrystals mixed solution was dropcasted onto the glass substrates to form blend films. The as-prepared sample films were covered with a 0.13 mm thin glass slide and encapsulated with epoxy glue in the glovebox before exposure to air.

Sample characterization

Transmission electron microscopy (TEM) measurements were carried out on a JEOL-2010F transmission electron microscope (JEOL) operating at an acceleration voltage of 200 kV. Scanning electron microscopy (SEM) images were recorded using a Leo Gemini 1530 VP SEM with an acceleration voltage of 3 kV. UV-vis diffuse reflection spectra were recorded on a Lambda 750 spectrophotometer equipped with an integrating sphere to collect all of the diffuse reflection from the samples.

Photothermal deflection spectroscopy (PDS)

Photothermal Deflection Spectroscopy (PDS) is a highly sensitive surface averaged absorption measurement technique. For the measurements, a monochromatic pump light beam produced by a combination of a Light Support MKII 100 W Xenon arc source and a CVI DK240 monochromator, is shone on the sample (thin-film on Quartz substrate) perpendicular to the plane of the sample, which on absorption produces a thermal gradient near the sample surface via non-radiative relaxation induced heating. Thus, resulting in a refractive index gradient in the area surrounding the sample surface. This refractive index gradient is further enhanced by immersing the sample in a deflection medium comprising of an inert liquid FC-72 Fluorinert® (3M Company), which has a high refractive index change per unit change in temperature. A fixed wavelength CW transverse laser probe beam, produced using a Qioptiq 670 nm fiber-coupled diode laser with temperature stabilizer for reduced beam pointing noise, was passed through the thermal gradient in front of the sample to produce a deflection proportional to the absorbed light at that particular wavelength. The signal is detected by a differentially amplified quadrant photodiode and a Stanford Research SR830 lock-in amplifier combination. Scanning through different wavelengths gives us complete absorption spectra.

Steady-state photoluminescence measurements

Photoluminescence spectra were measured by exciting the solid film using a diode laser (BrixX976 NB, 980 nm for upconversion; LDM405.100.CWA.L, 405 nm for downshifting) with a laser spot size of about 1 mm. The Spectra were recorded using a spectrometer (Andor, Shamrock SR-303i) integrated with a CCD detector (Andor, DU420A-BVF). For upconversion spectral measurements, a 900 nm short-pass filter was placed in front of the spectrometer to cut-off the scattering from the laser. The magnetic field dependent photoluminescence measurements were carried out using a spectrometer (Andor, Shamrock SR-303i) integrated with a CCD detector (Andor, DU420A-BVF) spectrometer with the samples placed in the center of an electromagnet (GMW, Model 3470).

Transient photoluminescence spectroscopy

Time-resolved photoluminescence measurements were obtained with a customized

phosphorescence lifetime spectrometer (Edinburgh, FSP920-C). A nanosecond optical parametric oscillator (OPO) pumped by a 3.8-ns-pulsed Nd:YAG laser (Ekspla, NT352) was used as the excitation source. The emission from the samples was collected at an angle of 90˚ to the excitation beam by using a pair of lenses.

Quantum yield measurements for upconversion emission

The quantum yield was measured using an integrating sphere method[34]. Samples were placed in an integrating sphere (Labsphere, 150 mm, internally coated with barium sulfate). A continuous-wave diode laser (BrixX976 NB, 980 nm) was used to excite the samples. The emission from the samples in the integrating sphere was collected by a spectrometer (Andor, Shamrock SR-303i) through an optical fiber. The signal was recorded by a CCD detector (Andor, DU420A-BVF). To avoid saturation of the detector by near-infrared signals, a near-infrared neutral density filter (Thorlabs, NENIR40B) was used to reduce the signal from the laser.

The quantum yield of upconversion emission was calculated by measuring the number of photons emitted versus the number of photons absorbed. In our quantum yield measurements, three experiments were carried out in an integrating sphere, and the total light intensity collected at the spectrometer was measured: (a) laser excitation with no sample, (b) laser excitation and sample emission with direct illumination of the sample, and (c) laser excitation and sample emission with indirect illumination of the sample. By integrating the excitation and emission signals, the upconversion efficiency was obtained as following calculations: the number of photons absorbed equals L_aA, where L_a is the excitation intensity in experiment a, and $A = 1-L_c/L_b$, where L_b and L_c are the excitation intensities in experiments b and c, respectively. The number of photons emitted equals $P_c-(1-A)P_b$, where P_b and P_c are the emission intensities in experiments b and c. Thus, the quantum yield is given by $PLQY = [P_c-(1-A)P_b]/L_aA$. This method accounts for all photons absorbed by direct excitation, indirect excitation via scattering in the integration sphere, and sample emission. The detailed quantum yield measurement and calculation can be found in a previous literature[34].

Transient absorption spectroscopy measurements

The samples were excited by a pump pulse and then probed at different delayed times using a

broadband probe pulse. Transient absorption spectra were recorded over short (500 fs to 6 ns) with a probe covering (500-850 nm, 750-1600 nm) and long (1 ns to 1 ms) time delays with a probe pulse covering 350-750 nm, 850-1020 nm. The short time (ps-TA) measurements were performed with a commercial transient absorption spectrometer (HELIOS, UltrafastSystems). A part of ultrafast pulses at ~790 nm from a regenerative Ti:sapphire amplifier system (Spectra Physics, Solstice) was used into pump a TOPAS-Prime (Light Conversion) to generate tunable pump pulses (355 nm~2600 nm). Another part of the laser source was introduced to a YAG crystal to generate a broadband probe pulse (800 nm~1550 nm). The probe light is delayed using a computer-controlled piezoelectric translation stage, and a sequence of probe pulses with and without the pump is generated using a chopper wheel on the pump beam. The pump and probe pulses were focused onto a ~0.5 mm^2 spot. The time resolution of the laser pulse was about 200 fs.

In long-time (ns-TA) measurements, an electronically controlled delay was employed. A separate frequency-doubled Q-switched Nd:YVO_4 laser (AOTYVO-25QSPX, Advanced Optical Technologies) is used to generate the pump pulses with a temporal breadth below 1 ns at 530 nm. The pump and probe beams overlap on the sample adjacent to a reference probe beam. This reference is used to account for any shot-to-shot variation in transmission. The sample is held in a 1 mm quartz cuvette, mounted into a holder. The beams are focused into an imaging spectrometer (Andor, Shamrock SR 303i) and detected using a pair of linear image sensors (Hamamatsu, G11608) driven and read out at the full laser repetition rate by a custom-built board from Stresing Entwicklungsburo. In all measurements, every second pump shot is omitted, either electronically for long-time measurements or using a mechanical chopper for short-time measurements. The fractional differential transmission ($\Delta T/T$) of the probe is calculated for each data point once 1000 shots are collected.

In pump-probe experiments as described above, differential transmission ($\Delta T/T$) signal in the TA spectra refers to features that define excited states. To identify different components from the transient absorption data, a genetic algorithm analysis was also used to distinguish different spectral species and the corresponding kinetics. In the pump-probe technique, a short light pulse (defined as ‘pump’) excites the sample, and the other pulse (defined as ‘probe’), which is broad in energy but short in time, interrogates the same spot after a time delay. The transmitted light from the probe is compared with and without the pump light and resolved by both the spectral wavelength and delay time. If there is a change in the spectra of the probe because of bleaching of the ground-state

transitions ('ground-state bleach'), stimulated emission, or excited-state absorption from one excited state to another, these will manifest as a change in the transmittance of the probe, ΔT. We recorded the signal normalized by the ground-state transmittance, ΔT/T, to facilitate comparison across experimental configurations.

We excited CPPOA at 355 nm to create singlet excitons (S_1) on the molecules and subsequently probed the evolution of the spectral features as a function of time. We note that the lanthanide ions have no transient absorption features and thus the entire response arises from the excited state features of CPPOA.

Data availability

The data underlying all figures in the main text and supplementary information are publicly available at DOI:XXXX (Data will be put on the Cambridge data repository, link to be added during proofs).

32. Wang, F., Deng, R. & Liu, X. Preparation of core-shell $NaGdF_4$ nanoparticles doped with luminescent lanthanide ions to be used as upconversion-based probes. *Nat. Protoc.* **9***,* 1634-1644 (2014).
33. Bogdan, N., Vetrone, F., Ozin, G. A. & Capobianco, J. A. Synthesis of ligand-free colloidally stable water dispersible brightly luminescent lanthanide-doped upconverting nanoparticles. *Nano Lett.* **11**, 835–840 (2011).
34. de Mello, J. C., Wittmann, H. F. & Friend, R. H. An improved experimental determination of external photoluminescence quantum efficiency. *Adv. Mater.* **9**, 230-232 (1997).

Acknowledgements This project has received funding from the European Research Council (ERC) under the European Union's Horizon 2020 research and innovation programme (grant agreement No 758826) and from the Marie Skłodowska-Curie grant agreement No 797619 (TET-Lanthanide project), No 748042 (MILORD project) and No 646176 (EXTMOS project). We acknowledge support from the Engineering and Physical Sciences Research Council (EPSRC) and the Winton Programme for the Physics of Sustainability, the Singapore Ministry of Education (Grant MOE2017-T2-2-110), Agency for

Science, Technology and Research (Grant A1883c0011), and National Research Foundation, Prime Minister's Office, Singapore under the NRF Investigatorship programme (Award No. NRF-NRFI05-2019-0003). R. D. acknowledges supports from the National Natural Science Foundation of China (51872256) and Zhejiang Provincial Natural Science Foundation of China (LR19B010002). Computational resources have been provided by the Consortium des Équipements de Calcul Intensif (CÉCI), funded by the Fonds de la Recherche Scientifique de Belgique (F.R.S.-FNRS) under Grant No. 2.5020.11 as well as the Tier-1 supercomputer of the Fédération Wallonie-Bruxelles, infrastructure funded by the Walloon Region under the grant agreement n1117545. L.N. acknowledges support from the Jardine Foundation.

Author contributions S.H., R.D. and A.R. designed the experiments. S.H., R.D., Z.Y. and B.Z. performed nanocrystal synthesis and film preparation. S.H., R.D., L.N., U.H., A.S. and S.A. carried out spectroscopic measurements. S.H., Q.G. and J.Z. contributed to transient absorption experiments and data analysis. H.T., A.P. and D.B. carried out theoretical calculations. H.X. prepared organic molecules. Z.H prepared organic molecules under the supervision of M.L.T. M.A. and A.S. performed PDS measurements. S.H., R.D., X.L. and A.R. wrote the manuscript. X.L. and A.R. supervised the project. All authors discussed the results and commented on the manuscript.

Competing interests The authors declare no competing financial interests.

Additional information

Supplementary Information is available for this paper at https://doi.org/xxx.

Correspondence and requests for materials should be addressed to A.R.; X.L. or R.D.

Reprints and permissions information is available at http://www.nature.com/reprints

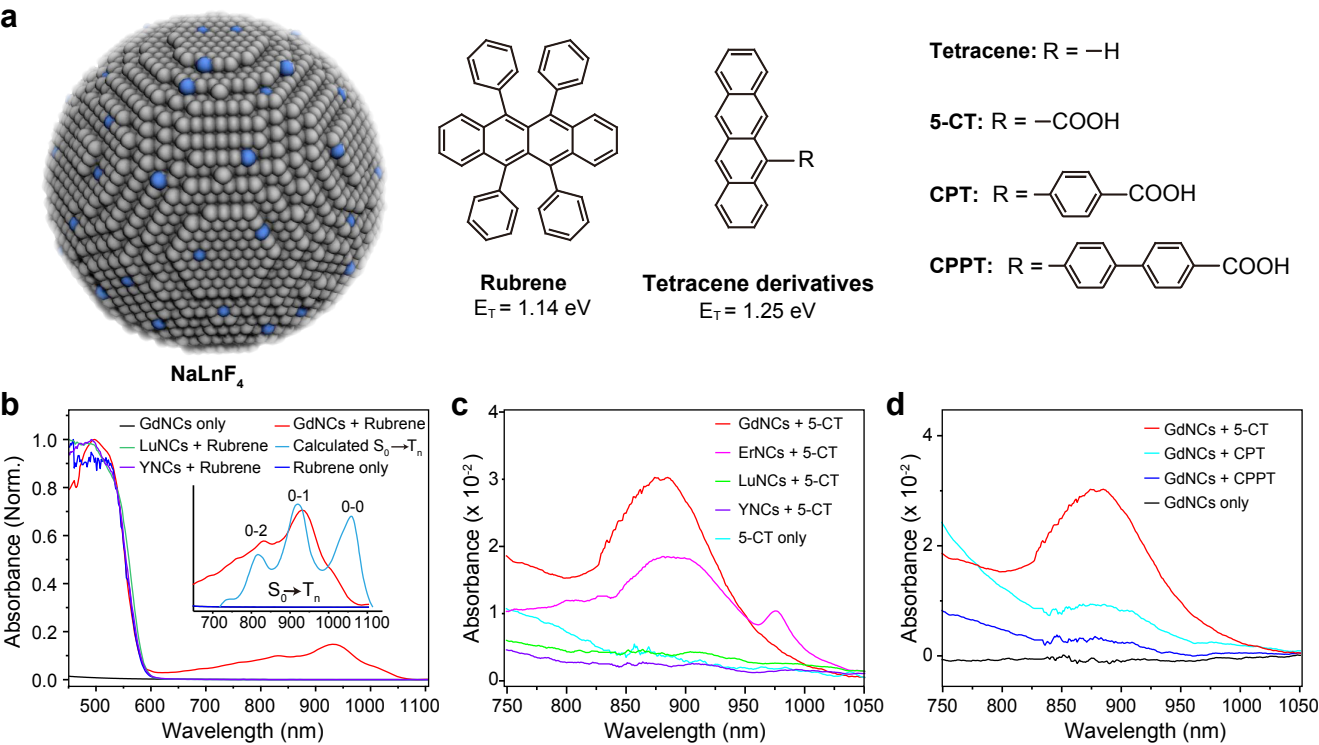
a
NaLnF4
Rubrene
ET = 1.14 eV
Tetracene derivatives
ET = 1.25 eV
R
Tetracene: R = −H
5-CT: R = −COOH
CPT: R = −C6H4−COOH
CPPT: R = −C6H4−C6H4−COOH
b
GdNCs only
GdNCs + Rubrene
LuNCs + Rubrene
Calculated S0→Tn
YNCs + Rubrene
Rubrene only
0-2
0-1
0-0
S0→Tn
Absorbance (Norm.)
Wavelength (nm)
c
GdNCs + 5-CT
ErNCs + 5-CT
LuNCs + 5-CT
YNCs + 5-CT
5-CT only
Absorbance (x 10-2)
Wavelength (nm)
d
GdNCs + 5-CT
GdNCs + CPT
GdNCs + CPPT
GdNCs only
Absorbance (x 10-2)
Wavelength (nm)

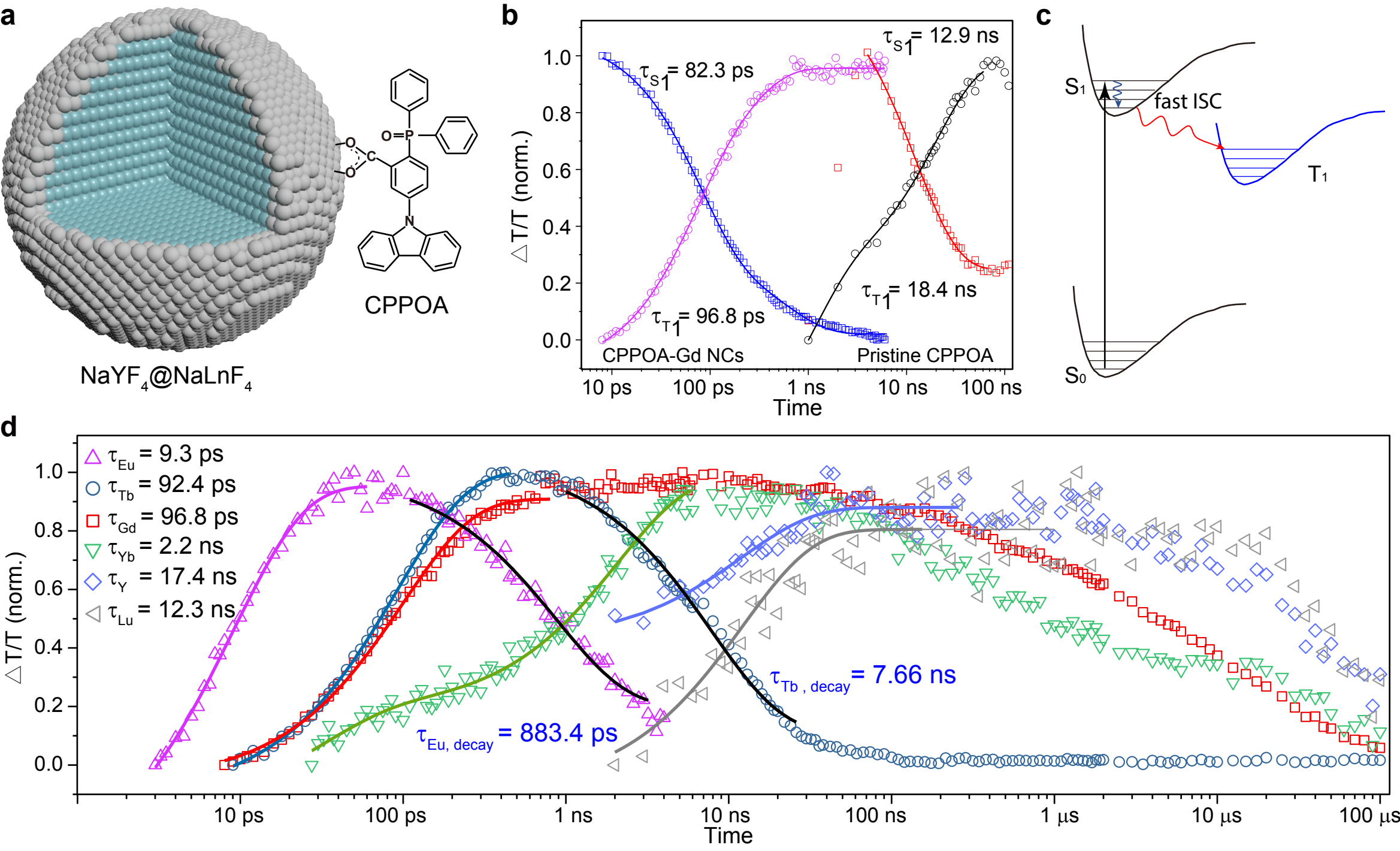
a
NaYF4@NaLnF4
CPPOA
b
τS1 = 82.3 ps
τS1 = 12.9 ns
τT1 = 96.8 ps
τT1 = 18.4 ns
CPPOA-Gd NCs
Pristine CPPOA
△T/T (norm.)
Time
10 ps
100 ps
1 ns
10 ns
100 ns
c
S1
fast ISC
T1
S0
d
τEu = 9.3 ps
τTb = 92.4 ps
τGd = 96.8 ps
τYb = 2.2 ns
τY = 17.4 ns
τLu = 12.3 ns
τEu, decay = 883.4 ps
τTb , decay = 7.66 ns
△T/T (norm.)
Time
10 ps
100 ps
1 ns
10 ns
100 ns
1 μs
10 μs
100 μs

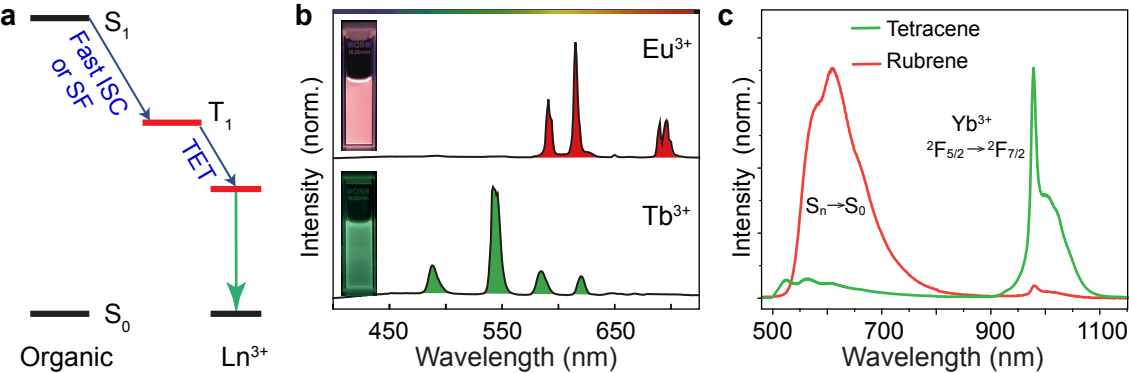
a
S1
Fast ISC
or SF
T1
TET
S0
Organic
Ln3+
b
Eu3+
Tb3+
Intensity (norm.)
450
550
650
Wavelength (nm)
c
Tetracene
Rubrene
Yb3+
2F5/2 → 2F7/2
Sn→S0
Intensity (norm.)
500
700
900
1100
Wavelength (nm)

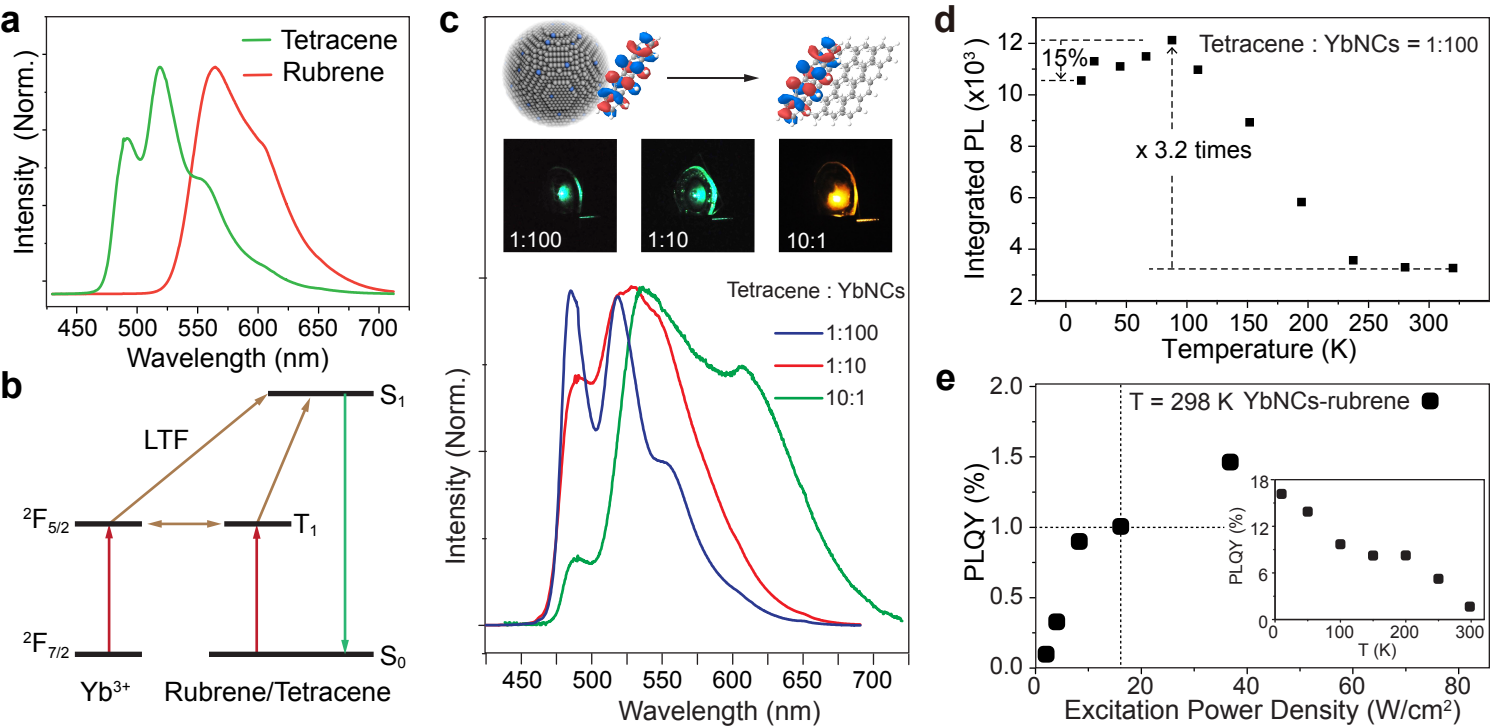
a
Tetracene
Rubrene
Intensity (Norm.)
450 500 550 600 650 700
Wavelength (nm)
b
S1
LTF
2F5/2
T1
2F7/2
S0
Yb3+
Rubrene/Tetracene
c
1:100
1:10
10:1
Tetracene : YbNCs
1:100
1:10
10:1
Intensity (Norm.)
450 500 550 600 650 700
Wavelength (nm)
d
Tetracene : YbNCs = 1:100
15%
x 3.2 times
Integrated PL (x10³)
0 50 100 150 200 250 300
Temperature (K)
e
T = 298 K YbNCs-rubrene
PLQY (%)
0 20 40 60 80
Excitation Power Density (W/cm²)
PLQY (%)
T (K)